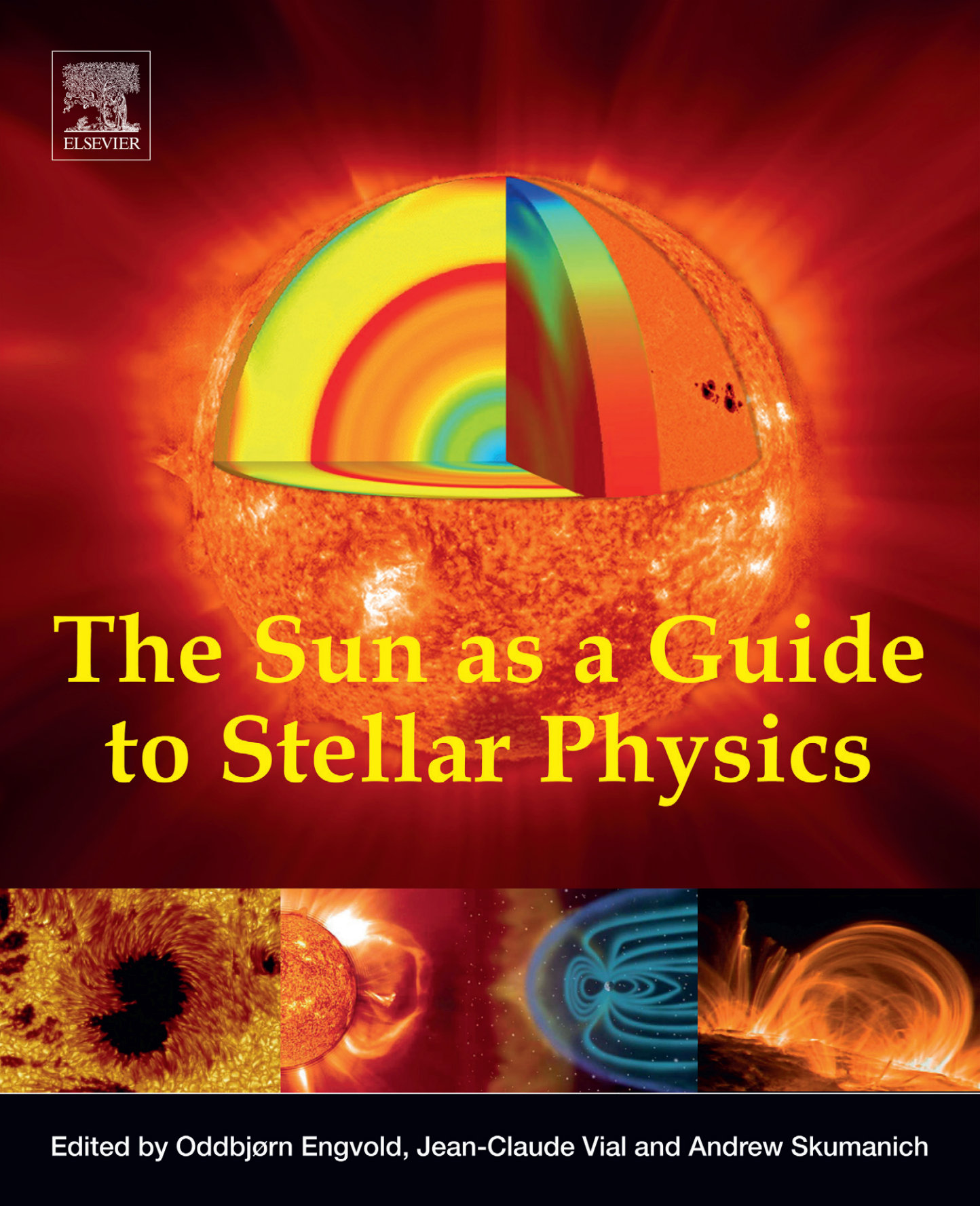
ELSEVIER
The Sun as a Guide to Stellar Physics
Edited by Oddbjørn Engvold, Jean-Claude Vial and Andrew Skumanich

The Sun as a Guide to Stellar Physics

This page intentionally left blank

The Sun as a Guide to Stellar Physics

Edited by

Oddbjørn Engvold
Professor emeritus, Rosseland Centre for Solar Physics, Institute of Theoretical Astrophysics, University of Oslo, Oslo, Norway

Jean-Claude Vial
Emeritus Senior Scientist, Institut d'Astrophysique Spatiale, CNRS-Université Paris-Sud, Orsay, France

Andrew Skumanich
Emeritus Senior Scientist, High Altitude Observatory, National Center for Atmospheric Research, Boulder, Colorado, United States

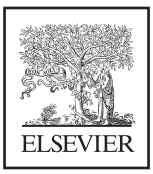

Elsevier
Radarweg 29, PO Box 211, 1000 AE Amsterdam, Netherlands
The Boulevard, Langford Lane, Kidlington, Oxford OX5 1GB, United Kingdom
50 Hampshire Street, 5th Floor, Cambridge, MA 02139, United States

Notices

Knowledge and best practice in this field are constantly changing. As new research and experience broaden our understanding, changes in research methods, professional practices, or medical treatment may become necessary.

Practitioners and researchers must always rely on their own experience and knowledge in evaluating and using any information, methods, compounds, or experiments described herein. In using such information or methods they should be mindful of their own safety and the safety of others, including parties for whom they have a professional responsibility.

To the fullest extent of the law, neither the Publisher nor the authors, contributors, or editors, assume any liability for any injury and/or damage to persons or property as a matter of products liability, negligence or otherwise, or from any use or operation of any methods, products, instructions, or ideas contained in the material herein.

Library of Congress Cataloging-in-Publication Data
A catalog record for this book is available from the Library of Congress

British Library Cataloguing-in-Publication Data
A catalogue record for this book is available from the British Library

ISBN: 978-0-12-814334-6

Publisher: Candice Janco
Acquisition Editor: Marisa LaFleur
Editorial Project Manager: Tasha Frank
Production Project Manager: Nilesh Kumar Shah
Designer: Miles Hitchen

Typeset by TNQ Technologies

(Main image) Anatomy of the Sun - Image of the Sun showing the Corona, Chromosphere and Photosphere, with a cut-away portion showing its interior, i.e. through the Convective and Radiative Zone into the Sun's Core. Credit: Bernhard Fleck, SOHO/ESA/NASA. (Left) An image of a sunspot group near solar disk center observed with the Swedish 1-m Solar Telescope on 15 July 2002. Credit: Göran B. Scharmer and Mats G. Löfdahl, Institute for Solar Physics, Stockholm University. (Middle) Composite image of the Sun showing a Coronal Mass Ejection heading for Earth's magnetic field and an artistic view of the Earth's bullet-shaped magnetosphere. Credit: ESA/NASA/SOHO/LASCO/EIT. (Right) Coronal loops seen above the solar edge with the TRACE (Transition Region and Coronal Explorer) instrument in the light of eight times ionized Iron (Fe 17.1 nm). Credit: Alan Title, Solar Astrophysics Laboratory, Lockheed Martin Advanced Technology Center, Palo Alto, California.

Contents

ATMOSPHERIC STRUCTURE, NON-EQUILIBRIUM THERMODYNAMICS AND MAGNETISM

This page intentionally left blank

List of Contributors

Thomas R. Ayres
University of Colorado, 389-UCB (CASA), Boulder, CO, United States

Gibor Basri
University of California, Berkeley, CA, United States

Sarbani Basu
Yale University, Department of Astronomy, New Haven, CT, United States

William J. Chaplin
University of Birmingham, School of Physics and Astronomy, Edgbaston, United Kingdom

Oddbjørn Engvold
Rosseland Centre for Solar Physics, Institute of Theoretical Astrophysics, University of Oslo, Oslo, Norway

Marianne Faurobert
University of Nice-Sophia Antipolis, Lagrange Laboratory, Nice, France

Petr Heinzel
Astronomical Institute, Czech Academy of Sciences, Ondřejov, Czech Republic

H.S. Hudson
School of Physics and Astronomy, University of Glasgow, Glasgow, United Kingdom; Space Sciences Laboratory, University of California, Berkeley, CA, United States

Neal Hurlburt
Lockheed Martin Advanced Technology Center, Palo Alto, CA, United States

Kiyoshi Ichimoto
Astronomical Observatory, Graduate School of Science, Kyoto University, Hida Observatory, Kurabashira Kamitakara-cho, Takayama-city, Japan; National Astronomical Observatory of Japan, Solar-C Project, Mitaka, Japan

Philip G. Judge
National Center for Atmospheric Research, High Altitude Observatory, Boulder, CO, United States

B.C. Low
High Altitude Observatory, National Center for Atmospheric Research, Boulder, CO, United States

Noé Lugaz
Space Science Center and Department of Physics, University of New Hampshire, Durham, NH, United States

A.L. MacKinnon
School of Physics and Astronomy, University of Glasgow, Glasgow, United Kingdom

Hardi Peter
Max-Planck-Institut für Sonnensystemforschung, Göttingen, Germany

E.R. Priest
School of Mathematics and Statistics, University of St. Andrews, St Andrews KY16 9SS, United Kingdom

Alexander I. Shapiro
Max-Planck-Institut für Sonnensystemforschung, Göttingen, Germany

Andrew Skumanich
Senior Scientist Emeritus, High Altitude Observatory, National Center for Atmospheric Research, Boulder, Colorado, United States

Sami K. Solanki
Max-Planck-Institut für Sonnensystemforschung, Göttingen, Germany; School of Space Research, Kyung Hee University, Yongin, Korea

Alan Title
Lockheed Martin Advanced Technology Center, Physics Department Stanford University Hanover Street, Palo Alto, California, United States

Jean-Claude Vial
Senior Scientist Emeritus, Institut d'Astrophysique Spatiale, CNRS-Université Paris-Sud, Orsay, France

Jack B. Zirker
National Solar Observatory, Sunspot, NM, United States

Preface

It has been said that solar physics is astronomy with a zoom lens. Modern observations of the Sun yield overwhelming complex details and dynamics of its variable corona, chromosphere, photosphere, and heliosphere, with ever-increasing spatial and temporal resolution. Observations and theory have led to the entirely new field of helioseismology. The Sun is generally assumed to represent a typical case of cool, magnetically active stars. However, it remains to be proven that the Sun qualifies fully as a "standard" star. Solar−stellar comparisons are mutually beneficial to both fields as well for a number of fields in physics.

The aim of *The Sun as a Guide to Stellar Physics* is to review and illustrate how "proxima solaris," where structures and time variabilities can be studied in detail from a full solar disk, have led to breakthroughs and progress in stellar science, as well as new discoveries and insight in associated areas of physics. This involves observations, theories, modeling, numerical simulations, instrumentation, and data processing. The 17 individual chapters represent various solar physics subfields. A brief overview of why interest in studying the Sun started and how is followed by more detailed descriptions and discussions of observational challenges and possibilities, a theoretical understanding, and modeling capacities behind the current level of insight and knowledge.

This book is prepared and written by solar and stellar physicists for a broader audience of interested astronomers, astrophysicists, and physicists.

The editors are most grateful to the 19 authors for their enthusiasm and willingness to contribute to the various specialized chapters. The insight and expertise of the chapter authors have been vital for the presentations of interpretations and understanding of frequently intricate interrelated solar phenomena. A multiauthor book will inevitably also risk repetitions in description and interpretation of particular phenomena in chapters covering related issues. Because authors often have their personal style and the book is aiming for a broad audience of readers, repeated descriptions and explanations of a discovery or idea as examined under different lights may be valuable to the reader.

The editors deeply thank R.M. Bonnet, J. Harvey, M. Knoelker, J. Leibacher, and S. Tremaine for their encouragements and B. Fleck for his help in this endeavor.

Oddbjørn Engvold
Jean-Claude Vial
Andrew Skumanich

This page intentionally left blank

CHAPTER

The Sun's Atmosphere

3

Alexander I. Shapiro[1], **Hardi Peter**[1], **Sami K. Solanki**[1,2]

Max-Planck-Institut für Sonnensystemforschung, Göttingen, Germany[1]*; School of Space Research, Kyung Hee University, Yongin, Korea*[2]

CHAPTER OUTLINE

1. INTRODUCTION

The solar atmosphere is usually defined as the outer, directly observable part of the Sun (in contrast to the deeper solar layers, which can be probed only indirectly with the help of helioseismology (see Chapter 4). In other words, the solar atmosphere gives birth to photons that leave the Sun in the form of sunlight. The solar atmosphere has a sharp lower edge in which the continuum radiation in the green part of the spectrum is emitted. Sometimes it is more precisely defined as the location at which optical depth unity is reached at 500 nm ($\tau_{500} = 1$). If photon escape is used as the definition, however, a deeper level should be used, such that almost no photons emitted below it make it into space. An optical depth of 10 is such a value. The two are separated by roughly 100 km on average, a tiny distance compared with the solar radius of roughly 7×10^5 km (which for the earth-based observer corresponds to the visible angular radius of about 1000 arcsec). By chance, the solar surface roughly coincides with the depth at which hydrogen ionization

The Sun as a Guide to Stellar Physics. https://doi.org/10.1016/B978-0-12-814334-6.00003-0

starts to set in (as the temperature rapidly rises with depth). The upper edge of the solar atmosphere is much more ambiguous to define. It extends out to a distance of several million kilometers, where it smoothly transitions into the solar wind, which is itself sometimes considered to be part of the solar atmosphere.

The solar atmosphere is traditionally divided into four layers, although considering these to be layers is now known to be only a very rough approximation. The deepest and coolest of these layers (with a temperature between approximately 6000−7000K at $\tau_{500} = 1$ and 4000−5000K at the top) is the solar photosphere, which emits most of its radiation as visible wavelengths. The photosphere is close to being in hydrostatical equilibrium with a pressure scale height of around 100 km. Consequently, solar matter quickly becomes opaque and the total vertical extension of the photosphere is just about 500 km (i.e., less than 0.1% of solar radius).

Above the photosphere lies the chromosphere, a layer with an average thickness of about 1500 km, where the temperature gradually rises to 10,000K in a spatially averaged sense. The chromosphere can be observed in the far UV, at millimeter wavelengths, and in the cores of the strong spectral lines at wavelengths in between. Because the temperature in the chromosphere is within a factor of 2 to that in the photosphere, the scale height of chromospheric gas is roughly the same as that of photospheric gas.

In a simple one-dimensional (1D) representation, the temperature above the chromosphere first jumps to more than 1 million K just within a 100-km-thick layer called the transition region and then flattens to form the solar corona. The transition region and corona can be observed in UV and at radio wavelengths of around 1 cm and longer X-rays.

We note that such a 1D representation of the solar atmosphere is a strong simplification: the solar atmosphere is strongly structured by various processes, with convection, magnetism, oscillations, and waves being the major structuring agents. Furthermore, the solar atmosphere is highly dynamic, so that at any given point in space, the properties of the atmosphere can change strongly with time.

2. OBSERVATIONS OF THE SOLAR ATMOSPHERE

In contrast to stellar physics, solar physics has been largely driven by the ability to resolve the features on the solar disk. In particular, high-resolution solar observations have made it possible to study the emergence and disappearance of solar magnetic fields directly as well as their sophisticated interaction with solar plasma. Consequently, such observations serve as a test bench for simulations of solar and stellar atmospheres.

High-resolution solar observations showed that in addition to a strong stratification with depth, the solar atmosphere has a rich and complex horizontal structure. The photospheric convective flows lead to the formation of granules, which are cellular features with a mean size of about 1000 km and a lifetime of about

10−20 min. Granules cover nearly the entire solar surface (with the exception of spots), so that at every moment there are several millions of granules on the Sun. Further inhomogeneities on the solar surface are caused by the magnetic field. Large concentrations of the magnetic field form dark sunspots, which consist of two parts: central umbral regions, which are the darkest parts of the sunspots with a predominantly vertical magnetic field, and surrounding penumbral regions, which are much lighter areas with an inclined magnetic field. The ensembles of smaller magnetic elements form bright network and faculae, which are most easily seen near the solar limb.

Over the last decade significant advances have been made with both ground-based (e.g., the detection of convective downflows in a sunspot penumbra with the Swedish 1-m Solar Telescope (Scharmer et al., 2011; Joshi et al., 2011a,b) and space-based (e.g., inversion of data from the Solar Optical Telescope aboard the Hinode satellite, which showed that solar internetwork consists of very inclined hG fields (Orozco Suárez et al., 2007)) solar observations. Another interesting strategy that allows observations with a large telescope in near-space conditions is to use balloon-borne solar observatories. Two flights of the SUNRISE (Solanki et al., 2010; Solanki et al., 2017), which is a balloon-borne solar Gregory telescope with a 1-m aperture, observing the Sun at a resolution of 50−100 km, resulted in a number of important discoveries. In particular, SUNRISE observations finally made it possible to resolve small-scale magnetic flux concentration in the quiet Sun (Lagg et al., 2010) and to study the migration and dispersal of such concentrations in intergranular lanes (Jafarzadeh et al., 2017).

Fig. 3.1 presents an overview of the solar atmosphere. Plotted are images showing the same field-of-view that cover an active region, sampling different temperature regimes corresponding to the photosphere, chromosphere, and corona. One interesting detail is that although a strong magnetic field (associated with the active region) is present over a large area (upper middle panel), only a small part of this field leads to the formation of sunspots (upper left panel). At the same time, the structure of the faculae/plage (in which the plage is the chromospheric counterpart of faculae) is similar to that of the magnetic field (compare the upper right panel with the upper middle panel). The lower left panel shows the transition region whereas the lower central and right panels sample the corona at different temperatures. One can clearly see the bright loops of gas in the corona connecting opposite magnetic polarities. These loops are thought to outline magnetic field lines.

3. THE SOLAR SPECTRUM

In this chapter we will focus on the disc-integrated solar spectrum. It is particularly important when considering the Sun as a star, because then no horizontal spatial information can be gleaned and only the flux as a function of wavelength or/and time is available. Interestingly, the distribution of energy in the solar spectrum is close to the spectral sensitivity of the human eye. Consequently, if not for the earth's

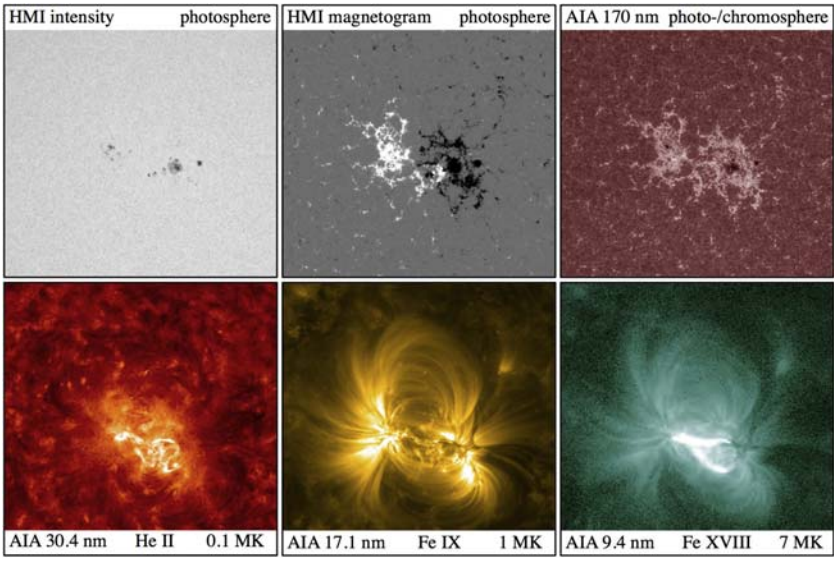

FIGURE 3.1

Overview of the solar atmosphere. The images show a 500 × 500-arcsec^2 part of the Sun (recall that the visible solar radius is about 1000 arcsec) with active region AR12139 recorded on Aug. 17, 2014 around 14:49 UT. Whereas the dark sunspots in photospheric intensity cover only a small fraction of the field of view, the magnetogram shows enhanced magnetic flux in a much larger area (black and white show opposite polarities). The intensity in the low chromosphere as seen in 170 nm pretty much correlates with the strong magnetic field, whereas the upper layers at hotter temperatures show the transition region and coronal structures connecting opposite polarities. For the latter panels, the main ions contributing to the wavelength channels are displayed along with the rough formation temperature.

Images are courtesy of the National Aeronautics and Space Administration/Solar Dynamics Observatory and the Atmospheric Imaging Assembly (AIA) and Helioseismic and Magnetic Imager (HMI) science teams.

atmosphere, the Sun would appear white to the human observer. However, because short-wavelength photons are better scattered in the atmosphere, the Sun appears to be yellow whereas the sky is blue (however, the true color of the Sun can still be glimpsed by looking at the white snow and clouds, which mix backscattered and transmitted solar photons).

In addition to the continuous spectrum (first spectrally analyzed by Isaac Newton), visible sunlight contains millions of absorption lines, first noticed by William Wollaston and studied in detail by Joseph Fraunhofer and later called Fraunhofer lines.

A significant milestone in solar spectroscopy was reached with the introduction of the Fourier Transform spectrometer (Brault, 1985) at the McMath-Pierce Solar Facility at the National Solar Observatory on Kitt Peak in the early 1980s (see Doerr

et al., 2016, for a historical overview of available solar spectra). Since then, several versions of the Kitt Peak spectral atlases have been released (Kurucz, 1984; Kurucz, 2005a; Wallace et al., 2011).

Fig. 3.2 presents the first version of the Kitt Peak Solar Flux Atlas by Kurucz et al. (Kurucz, 1984). The large number of absorption lines is striking; it is so

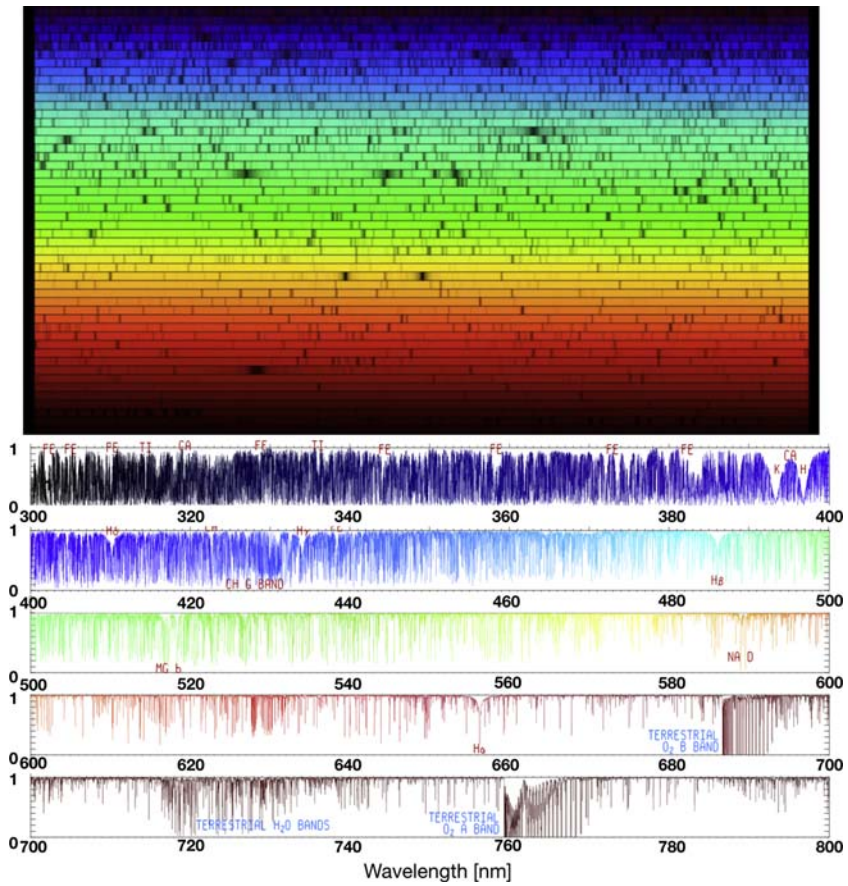

FIGURE 3.2

Kitt peak solar flux atlas (Kurucz, 1984) Upper panel: an artificially created image representation. Each of the 50 slices covers 6 nm; together, they span the complete spectrum across the visual range from 400 to 700 nm. The wavelength increases from left to right along each strip, and from top to bottom. Lower panel: a graphical representation of the same atlas between 300 and 800 nm. The flux values at every wavelengths are normalized to the local continuum value.

Source: The image in the upper panel as well as the caption are adapted from https://www.noao.edu/image_gallery/html/im0600.html. Credits: N.A. Sharp, National Optical Astronomy Observatory/National Solar Observatory/Kitt Peak Fourier Transform spectrometer/Association of Universities for Research in Astronomy/National Science Foundation. The figure in the lower panel is taken from http://kurucz.harvard.edu/sun/fluxatlas2005/.

huge that whereas current linelists used for modeling and interpreting solar spectra contain more than 100 million atomic and molecular lines, many if not most of the lines are so strongly blended that they cannot be identified (Kurucz, 2005b). Another important detail that makes solar spectra look different from spectra of hotter stars is the absence of the Balmer jump around 364.6 nm. It is practically invisible in the solar spectrum because the dominant source of the continuum opacity in the solar photosphere is the negative hydrogen ion. A small continuum jump introduced by neutral hydrogen (see, e.g., Fig. 1 from Shapiro et al., 2015) is completely masked by the Fraunhofer lines. The role of neutral hydrogen in the continuum opacity increases with the effective temperature and the Balmer jump becomes one of the most dominant features in the spectra of A stars. Interestingly, because the opacity of negative hydrogen depends only weakly on the wavelength, the solar spectrum is much more similar to the Planck's law than spectra of hotter stars. The main deviations of the solar spectrum from the Planck's law in the visible spectral domain are caused by the Fraunhofer lines.

Fig. 3.2 identifies the main physical mechanisms responsible for the creation of the photons forming sunlight. In the UV these are scattering and thermal emissions of photons in spectral lines. The number of lines decreases toward longer wavelengths where continuum photons also increasingly escape the atmosphere. Consequently, starting from approximately 500−550 nm, most of the photons come from the continuum and are produced during the recombination of neutral hydrogen with electrons to form the negative hydrogen ion.

Whereas the main source of line opacity in the solar atmosphere is atomic lines, the solar spectrum also contains several strong molecular features. The most prominent among them are the CN violet system at about 380 nm and the CH G-band at about 430 nm. Interestingly, approximately a quarter of solar brightness variability on the timescale of the 11-year magnetic activity cycle comes from the molecular lines (Shapiro et al., 2015). The contribution of molecular lines to the spectrum increases for stars cooler than the Sun, and in the spectra of sunspots and pores, comparatively dark and hence cool concentrations of magnetic flux. With a decrease in the effective temperature, first lines of carbon-based diatomic molecules become more pronounced and then (for temperatures below 4500K, i.e., in M stars and in sunspot umbrae, i.e., the darkest parts of sunspots) the main contribution to line opacity shifts to molecules composed of α-elements, in particular TiO and MgH (see Fig. 3 from de Laverny et al., 2012).

The vast number of lines in the spectra of stars with near-solar temperature and cooler is an asset for detecting planets with the radial velocity (RV) method (which currently accounts for roughly half of all discovered exoplanets (http://exoplanets.eu). The number of spectral lines decreases with the effective temperature and the lines also become broader owing to the faster rotation of these stars (because they are younger than the Sun and consequently did not undergo such strong magnetic braking). Consequently, it becomes difficult to determine the Doppler shift and most of the RV exoplanets were discovered around stars later than spectral type F6 (Hatzes, 2016).

Interestingly, spectral lines below 180 nm are observed in emission whereas most of the lines above this threshold are observed in absorption. This happens because of the temperature inversion in the solar atmosphere: the temperature first decreases with height in the photosphere, reaches a minimum of about 4000−5000K, and then starts to increase in the chromosphere. The pseudocontinuum at about 180 nm is formed around the temperature minimum so that lines below 180 nm are chromospheric (and seen in emission) whereas lines above 180 nm are photospheric (and seen in absorption). Interestingly, there is also a second spectral window to observe the atmospheric layers around the temperature minimum: the opacity in the far infrared is dominated by the negative hydrogen free-free absorption, which rapidly increases with wavelength (as λ^2). Consequently, the chromosphere becomes optically thick at about 150 μm and similar to the UV case, this threshold separates photospheric and chromospheric photons.

4. PHYSICS OF THE PHOTOSPHERE/CHROMOSPHERE

4.1 ONE-DIMENSIONAL MODELS

We start with a brief overview of simplified 1D models that describe the solar atmosphere as a plane-parallel structure. Although they are obvious simplifications, these models had an important role in understating some of the physical processes in the solar atmosphere.

The 1D models can be divided into two main classes. The first class encompasses models with a temperature structure calculated assuming radiative equilibrium (hereafter RE models), i.e., assuming that the only source of energy transport is radiation. Because this is not correct close to the solar surface, they are often corrected for the transport of mechanical energy by convection, which is parameterized through the mixing length theory (Böhm-Vitense, 1958) or overshooting approximation (Castelli et al., 1997). RE models can be calculated for stars with arbitrary fundamental parameters (i.e., effective temperature, metallicity, and surface gravity), and although they are gradually superseded by 3D magnetohydrodynamic approximation (MHD) models (Tremblay et al., 2013; Beeck et al., 2013), they are still routinely used in stellar modeling. The most prominent examples of RE models are ATLAS9 and ATLAS12 (Kurucz, 2005c), MARCS (Gustafsson et al., 2008), and PHOENIX (Husser et al., 2013).

A strong drawback of the RE models is that they cannot describe the temperature rise in the chromosphere as well as structures of the bright magnetic features (such as network and faculae). In the solar case, such a drawback is overcome by the second class of model, namely the semiempirical models (hereafter, SE models). The atmospheric temperature structure in these models is empirically determined from the observed solar spectrum and its center-to-limb variation. Although the SE models do not directly rely on the assumption of RE, their photospheric

stratification, in particular in the quiet Sun (as well as in sunspots) often appears to be close to RE (Fontenla et al., 1999; Rutten, 2002).

Most of the SE models still used nowadays (Avrett, 1985; Fontenla et al., 1993; Fontenla et al., 2015 and references therein) stem from the work by Vernazza, Avrett, and Loeser (VAL) (Vernazza et al., 1981). They used a set of observations to create a series of models for several brightness components of the quiet Sun. For example, they used spectra of the continuum in the 135- to 168-nm range (where the transition from emission to absorption lines happens) (see Section 3) to constrain the properties of atmospheric layers around the temperature minimum region.

The temperature stratifications of VAL models are plotted in Fig. 3.3. Six models that differ quantitatively from each other but are qualitatively similar are meant to represent regions with different amounts of magnetic flux, from the dark parts of

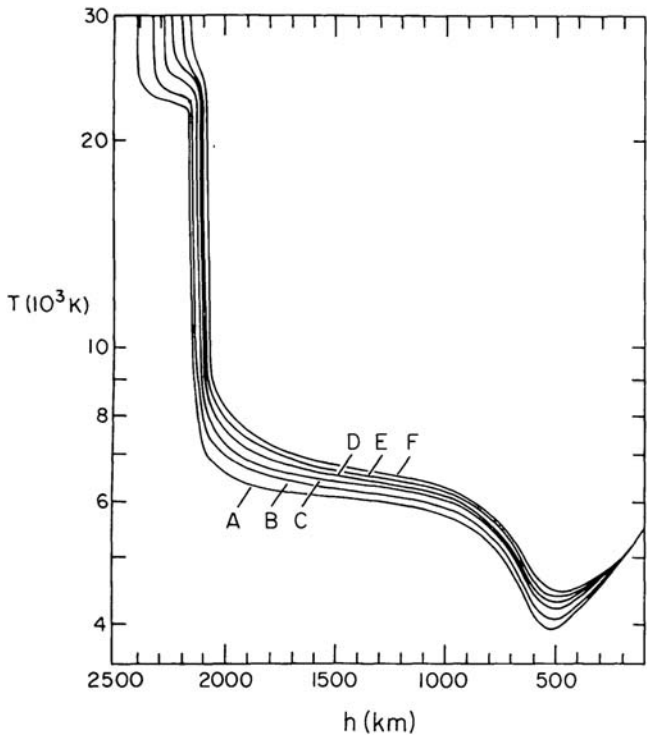

FIGURE 3.3

Temperature as a function of height for a Vernazza, Avrett, and Loeser (Vernazza et al., 1981, Avrett, 1985) set of semiempirical solar model atmospheres: a dark point within a supergranule cell interior (A), the average supergranule cell interior (B), the average quiet Sun (C), the average network (D), a bright network element (E), a very bright network elements (F).

From Vernazza, J.E., Avrett, E. H., Loeser, R., 1981. ApJS 45 635. http://adsabs.harvard.edu/abs/1981ApJS...45..635V.

the interiors of supergranule cells in the quiet Sun to the brightest network elements (even brighter plage regions are found within active regions). Basically, these regions differ in the degrees of their coverage by small-scale magnetic flux tubes (which are a widely used description of the magnetic flux concentrations on the solar surface) (see, e.g., Solanki et al., 1993 for a detailed review) (Solanki et al., 2006). Together with the granulation, the magnetic flux tubes are the main structuring agents in the photosphere. Furthermore, they have an important role in structuring and energizing the entire solar atmosphere, providing a channel for the transport of energy from the convection zone to the outer atmosphere.

Independently of the size, all magnetic flux tubes have a roughly equally strong field of 1−1.5 kilogauss (kG) (which is a mean field, i.e., averaged over their cross-section) sufficient to inhibit the convection and energy flux associated with it significantly. Consequently, the flux tubes with a diameter larger than a 1000 km are visible as dark pores and the even larger ones as sunspots. In contrast, smaller flux tubes (often called magnetic elements) form bright points, ensembles of which can be observed as network and faculae. This is because the optical depth unity surfaces within magnetic flux concentrations are found at lower layers of the Sun owing to the horizontal pressure balance with their surroundings. This lowering of the solar surface within magnetic flux concentrations is called the Wilson depression. Because near the solar surface the temperature increases rapidly downward, the flux tubes are surrounded by hot walls (Fig. 3.4) (Solanki et al., 2013). This leads to two effects that define the spectral contrasts of magnetic elements relative to the surrounding quiet regions: (1) interiors of flux tubes are heated by radiation from the hot walls, and (2) the hot walls can be directly seen when magnetic elements are observed away from the disc center. In particular, the second effect is responsible for the center-to-limb variation of contrasts of magnetic elements: they are barely distinguishable from the quiet regions when observed close to the disk center (because hot walls are not visible) and appear bright toward the limb. As a result, the network and active-region faculae are mainly visible as bright structures in the continuum at visible wavelengths (e.g., in white light) mainly close to the solar limb. The photospheric temperature stratification of six brightness components in Fig. 3.3 is produced to emulate this purely 3D effect of hot walls' visibility within the constraints of 1D geometry. Namely, the temperature structures of all six models are similar in the lower photosphere (where continuum radiation emitted near the solar disk center is formed) and start to diverge with height, at least below the temperature minimum (where the radiation emitted away from the disk center is formed).

The decrease in the photospheric temperature with height in all components can be easily understood in terms of RE: such a temperature gradient is needed to transfer the radiative energy through the photosphere. On the contrary, the increase in the temperature with height in the chromosphere (i.e., above the temperature minimum) cannot be explained under the assumption of RE: there must be a nonradiative heating mechanism. For the quiet Sun, the necessary energy is transported by acoustic waves generated in the upper convection zone and traveling upward through the

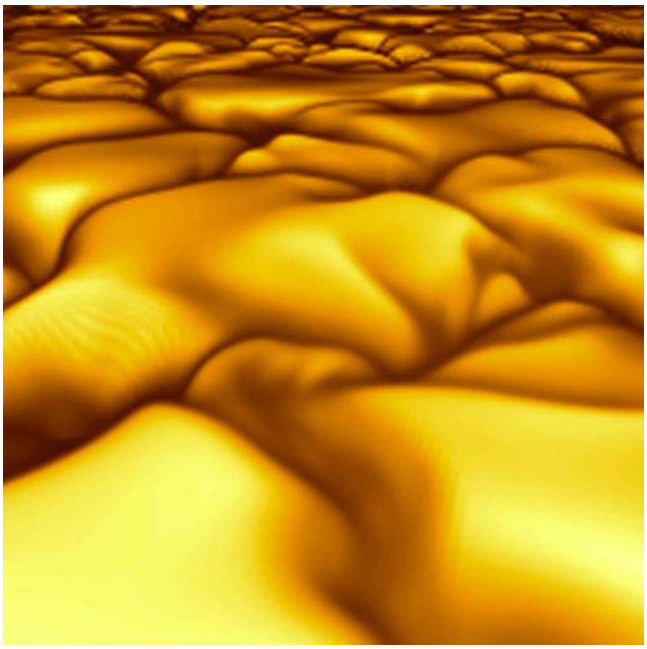

FIGURE 3.4

The emergent intensity from a magneto-convection simulation observed from a vantage point corresponding to it being near the limb.

Still from a movie by Mats Carlsson taken from:Nordlund,A°., Stein, R.F., Asplund, M., 2009.

solar atmosphere (Solanki et al., 2002; Werner et al., 2003). The amplitude of the waves increases with decreasing gas density in the chromosphere and they start to form shocks in the layers above the temperature minimum, heating them. Consequently, the temperature in the chromosphere, on average, steeply increases between the temperature minimum and layers at $h \approx 1000$ km, although the actual temperature is strongly perturbed in space and time. At these layers, the ionization of hydrogen starts. It absorbs a lot of the energy released within the chromosphere, dramatically increasing its heat capacity. Consequently, the temperature profile flattens, forming the plateau. At $h \approx 2000$ km, the number density of neutral hydrogen is no longer sufficient to absorb all of the energy from the shock waves. Furthermore, a significant amount of energy is transported to these layers from the solar corona by thermal conduction. As a result, the temperature suddenly jumps by more than 10,000K. Then the chromosphere starts to be transparent for Lyman-α radiation, which effectively cools it down again, forming the second temperature plateau at $20-30/c \cdot 10^3$ K seen in the models in Fig. 3.3.

The calculations of the spectra emergent from 1D models are relatively fast, and with increasing computer capacity more and more sophisticated radiative transfer effects can be taken into account (Werner et al., 2003). Of particular importance are the effects caused by the deviations from the local thermodynamic equilibrium (for non-LTE effects, see Section 9.1 of Hubeny and Mihalas (Hubeny and Mihalas, 2014) for a detailed review). They arise when the coupling between photons and atmospheric gas (enforced by the inelastic collisions) weakens and photons created in one part of the atmosphere affect the conditions (e.g., the degree of ionization) in nearby parts. In this case, atomic and molecular populations can no longer be calculated with the Saha−Boltzmann equation and instead a system of statistical balance equations has to be solved simultaneously with the radiative transfer equation. The non-LTE effects are present when the assumption of the detailed balance, i.e., that any process in the atmosphere is exactly balanced by the inverse process, is broken.

The non-LTE effects are especially strong in the chromosphere where the gas density and consequently collision rates are too small to maintain LTE. Because of the strong temperature gradient, they also have an important role in the middle and upper photosphere: UV photons emergent in the lower and hotter parts of the photosphere penetrate into the higher and cooler layers and cause excessive (relative to the one given by the Saha−Boltzmann equation) iron and other metals ionization (Short and Hauschildt, 2009).

The 1D SE models describe only some of the aspects of the highly inhomogeneous and dynamical 3D solar atmosphere and are by far not as reliable for the diagnostics of atmospheric properties as modern 3D models, at least in the photosphere (Koesterke et al., 2008; Uitenbroek and Criscuoli, 2011) and more recently also in the chromosphere (de la Cruz Rodríguez et al., 2016; Ermolli et al., 2013). At the same time, they yield a convenient way of interpolating from a specific set of spectral measurements (e.g., emergent intensities from quiet Sun and magnetic features measured at some sparse grids of wavelengths and position angles, i.e., distances to the solar disc center) to the entire parameter space of wavelengths and position angles. Consequently, SE models are still used extensively in studies of solar irradiance variability (see, e.g., reviews by Ermolli et al. (Ermolli et al., 2013) and Solanki et al. (Solanki et al., 2013)) for providing contrasts of magnetic features relative to the quiet Sun as functions of the wavelength and position angle.

Because of the lack of data, the SE approach has not been widely used for stellar atmospheres, but the main concept behind the approach proved to be useful in stellar physics as well. For example, Liseau et al. (Liseau et al., 2013) observed the spectrum of α Cen A in the far infrared wavelength range, where the solar temperature minimum can be observed (see Section 3). Similar to the solar case, they found that the brightness temperature has a minimum at around 160 μm and $T_{\min} = 3920 \pm 375$K. This became the first direct measurement of a temperature minimum on a star other than the Sun.

4.2 THREE-DIMENSIONAL MODELS

The 3D models of the solar atmosphere usually rely on the MHD, which describes plasma as a fluid and combines equations of hydrodynamics (i.e., the continuity equation, the equation of motion, and the energy equation) with the induction equation for the magnetic field (see a detailed description of the MHD equations in Chapter 7). There are two main classes of 3D magnetohydrodynamic models: "idealized" and "realistic." Idealized studies assume a fully ionized, ideal plasma and ignore radiative transfer (so that the energy is only transferred by thermal conduction and advection) (see, e.g., review by Schüssler et al. (Schüssler et al., 2001)).

The real breakthrough has been the realistic 3D simulations of the lower solar atmosphere. Two main features of the realistic simulations are that they account for (1) partial ionization and (2) the radiative transfer of energy in 3D. The former is crucial in the upper convective zone because the ionization energy dominates the convective energy transport whereas the latter takes over from convection as the dominant energy transport mechanism in the photosphere and determines the cooling of the solar atmosphere.

The effects of partial ionization are taken into account via the equation of state (EOS), which gives the main thermodynamical quantities (e.g., pressure, electron concentration, and internal energy) as functions of temperature and density. The EOS can be either ideal and rely on the Saha ionization equation and chemical equilibrium, or nonideal, e.g., include many-body effects, electron degeneracy, and corrections owing to Coulomb interaction (see the detailed discussion and intercomparison of various EOS in (Vitas and Khomenko, 2015)).

The treatment of the radiative transfer is relatively simple at depths below the surface. The radiation is almost isotropic and trapped there, so that the diffusion approximation can be applied (Hubeny and Mihalas, 2014 p. 374). At the same time the photons can escape in the solar atmosphere and a more sophisticated treatment of the radiative transfer is needed. Generally, the solution of the radiative transfer is the most time-consuming part of the realistic simulations. The main numerical problem here is accounting for the millions of atomic and molecular lines that affect the structure of the solar atmosphere via the line cooling and back-warming effects (see Sections. 4.2 and 5.3 of the doctoral thesis of Alexander Vögler). The most direct way to take these effects into account is to solve the radiative transfer on a fine frequency grid. This is feasible in static 1D calculations but it becomes unbearably time-consuming in 2D and 3D dynamical simulations. One way to solve this problem, which is now routinely applied in most MHD codes, is to sort all frequency points into a small number of groups (4−12 are typically used) according to the formation heights of radiation at these frequencies. Then the group-integrated intensity values are calculated assuming gray radiative transfer within each of the groups (Nordlund, 1982; Vögler et al., 2005).

Another important sophistication is non-LTE effects, which are especially strong in the chromosphere where collision rates drop (see Section 4.1). In particular, non-LTE effects influence the cooling rates in spectral lines and the EOS (owing to

non-Saha ionization). Over the past few years, realistic simulations started to account for various non-LTE effects, e.g., the effects of scattering in spectral lines and the continuum (Hayek et al., 2010), non-equilibrium hydrogen and helium ionization (Golding et al., 2016), and non-LTE radiative cooling in chromospheric hydrogen, magnesium, and calcium lines (Carlsson and Leenaarts, 2012).

In contrast to the parameterized consideration in 1D models, 3D MHD models make it possible to simulate the structure and dynamics of the magnetic field and granulation directly, as well as the interplay between them. In particular, modern realistic simulations are capable of reproducing granules: areas of hot upflows with a typical size of 1000 km surrounded by cooler lanes of downflowing gas. Fig. 3.4 shows the granulation pattern simulated by Carlsson et al. (Carlsson et al., 2004). The figure illustrates a remarkable property of the solar surface: it has an uneven 3D structure. This can be explained by the strong sensitivity of the negative hydrogen ion concentration (which is the main source of the opacity in the lower photosphere) to temperature (see Section 3). The concentration of negative hydrogen ions is lower in the cooler downflowing lanes (owing to a drop in the free electron concentration there) than in the warmer upflowing interiors of granules. Consequently, the surface of unity optical depth is approximately 35 km higher in upflows than in downflows in nonmagnetic regions (Frutiger et al., 2000). Along the same line, concentrations of the strong magnetic field are lower than the nonmagnetic solar surface by up to 350 km owing to the Wilson depression (see Section 4.1).

Of particular relevance to stellar studies is that one of the best observational constants in simulations of solar convection comes from the spatially unresolved observations of the Fraunhofer lines (see, e.g., a detailed discussion in Nordlund et al., 2009). This is because whereas convective instability stops just below the solar surface, it overshoots into the solar photosphere, affecting the shapes and widths of the Fraunhofer lines. Fig. 3.5 illustrates the high quality of the agreement between spectra computed using realistic simulations and those with observations. Namely, it shows a comparison between the Kitt Peak solar spectral atlas (see Section 4.1) and a spectrum computed with the SPINOR code (Frutiger et al., 2000) using a piece of the solar atmosphere simulated with the *Max-Planck*-Institut für Sonnensystemforschung/University of Chicago Radiative MHD (MURaM) (Vögler et al., 2005) code. The agreement between the two spectra is remarkably good for both the UV region with numerous OH and atomic lines (upper panel) and the visible spectrum dominated by several intermediate strength Fe lines (lower panels). Naturally, the comparison between simulated and observed spectra is not limited to the solar case. Numerous studies have shown that realistic simulations of stellar atmospheres give velocity fields consistent with observed line bisectors and widths (Allende Prieto et al., 2002; Ramírez et al., 2009; Trampedach et al., 2013).

Convective motion in the photosphere and in subphotospheric layers has a crucial role in defining the structure of the small-scale photospheric magnetic concentrations (i.e., bright points, network, and faculae). Dynamo action in the solar convective envelope (and probably in the overshoot layer at its base) produces a continuum of

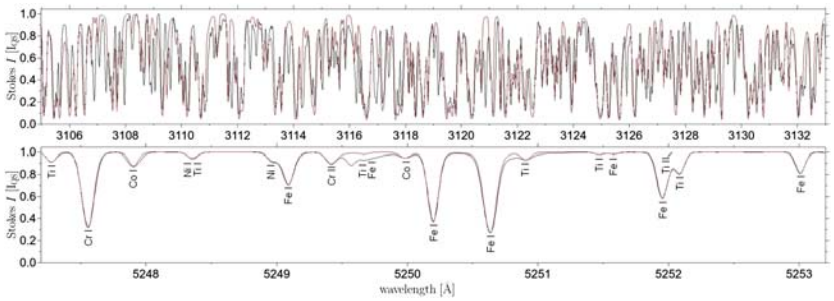

FIGURE 3.5

Excerpts from a National Solar Observatory spectral atlas of the quiet Sun at the center of the solar disc (*black lines*), spatially averaged synthetic spectra (*red lines*) for the part of the OH band plus atomic lines around 311.8 nm (upper panel) and for the spectral region around the Fe I line at 525.02 nm, often used in solar physics because of its large magnetic sensitivity (lower panel).

magnetic structures of different sizes. These rise through the visible solar surface and into the atmosphere in the form of loops. At the surface itself, they are visible as ensembles of magnetic flux tubes with mixed polarities. Convective motion quickly drags magnetic flux tubes into the intergranular lanes, and then toward the supergranule boundaries (on timescales of days) (Stein, 2012). At the same time, magnetic flux tubes are canceling (if of opposite polarity), dissolving, fragmenting, and forming again (so that Schrijver et al. (1998) estimated that the flux in the magnetic network is renewed every 40 h). Consequently, the final structure of the photospheric magnetic field is determined by the balance between the emerging field and the rate at which the field is dragged by the convective motion, with most of the magnetic flux tubes being concentrated in the supergranule boundaries.

The structure of the magnetic field in the quiet Sun changes dramatically in the chromosphere. The pressure in the hotter magnetic flux tubes (see Section 4.1) decreases slower than in the cooler surroundings. Consequently, magnetic flux tubes cannot be confined by the external gas at layers above about 700−1000 km (Solanki and Hammer, 2002). As a result, large patches of an almost horizontal field known as a magnetic canopy are formed. Above this height, the solar atmosphere is completely filled by magnetic field and also energetically dominated by it, i.e., the outer atmosphere of the Sun is a magnetosphere.

Simulations of the solar atmosphere have reached a level of realism that allows predictions to be made about the structure of the atmosphere of other cool stars. Unlike earlier, purely hydrodynamic simulations (Nordlund and Dravins, 1990; Freytag et al., 1996; Asplund et al., 1999), they now also include magnetic field. Fig. 3.6 shows maps of the vertically emerging bolometric intensity (upper panel) and of the vertical component of the magnetic field simulated by Beeck et al. (2015) with the MURaM code for main sequence stars of F3, G2 (i.e., solar case), and K0 spectral classes. The

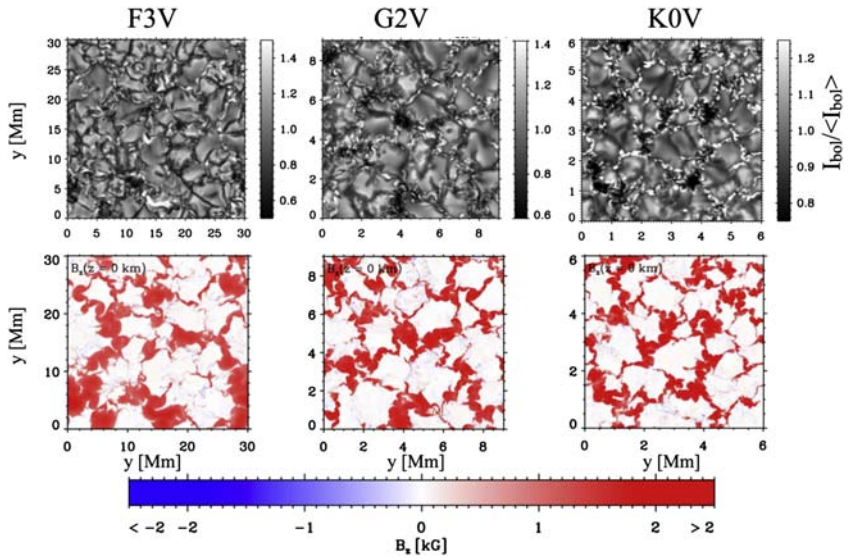

FIGURE 3.6

Maps of the vertical bolometric intensity for *Max-Planck*-Institut für Sonnensystemforschung/University of Chicago Radiative magnetohydrodynamic approximation simulations of F3V, G2V, and KOV stars (upper panels) and corresponding maps of the vertical component, B_z, of the magnetic field at $z = 0$, the average geometrical depth of the optical surface (lower panels). For improved image contrast, brightness in the upper panels saturates at the values indicated by the gray scales on the right of each panel. The initial magnetic field was unipolar, vertical with a uniform field strength of 500 G.

The figure is adapted from Beeck B., Schüssler M., Cameron R.H., et al. Three-dimensional simulations of near-surface convection in main-sequence stars. III. The structure of small-scale magnetic flux concentrations. Astron. Astrophys. 2015; 581:A42. doi:10.1051/0004−6361/201525788. 1505.04739.

horizontal size of the simulations has been scaled with the expected granule sizes. One can see that independently of the spectral class, the convective motion drags the magnetic field to the convective downflows in the intergranular lanes where a field up to several kG is formed. The locations of a strong field coincide with regions of enhanced or reduced intensity. The intensity contrasts of the magnetic elements notably depend on the spectral type (decreasing toward cooler stars) (see detailed explanations of this effect in Beeck et al., (2015)).

5. PHYSICS OF THE CHROMOSPHERE/CORONA

One major difference between the photosphere and the corona is found in the roles the plasma and the magnetic field have, which are characterized by the ratio of the

energy densities of the gas and the magnetic field, the plasma-β. On average, in the photosphere (outside sunspots) β is above unity, i.e., the thermal energy dominates, whereas in the corona β is below unity and the magnetic field dominates energetically. This causes the radically different appearance of the two atmospheric regimes. In the photosphere, the (overshooting) convection structures the atmosphere, e.g., resulting in granules, and through the interplay with the magnetic field convection creates small flux tubes with field strengths of up to kG (Lagg et al., 2016). In contrast, in the corona the magnetic field is basically filling space and heated plasma is trapped along the magnetic field, forming coronal loops. These are best seen in emission from plasma at around 10^6K, e.g., visualized in filter images near 171 Å that are dominated by emission lines from Fe IX (Fig. 3.1). Because the magnetic field dominates in the corona, the gas does not alter the magnetic field significantly, and thus the plasma outlines magnetic field lines in a way similar to that of iron fillings in a school experiment.

If, in general, the gas dominates in the photosphere and the magnetic field does so in the corona, there must be an interface where they roughly balance. This is the case somewhere in the chromosphere. The exact height where this happens depends on the average magnetic flux density of the region. This transition is why this atmospheric regime is so interesting for the magnetic connection from the surface to the upper atmosphere. Besides, the chromosphere is challenging with respect to a correct description of its physics. At low temperatures (Fig. 3.3), the gas is only partially ionized, and combined with the density and collisional coupling, processes such as the Hall effect and ambipolar diffusion become important. This basically accounts for the increased slippage of the magnetic field through the plasma, or vice versa (see Section 5.4). Together with the requirement to treat chromospheric lines under non-LTE conditions (see Section 4.1), these effects make the chromosphere the most challenging regime in the solar atmosphere in terms of modeling and interpretation.

Between the chromosphere and the corona lies the transition region, in which the temperature jumps from a few 10,000K to nearly a million K. In 1D models the transition region is extremely narrow, having a thickness well below a few dozen km. Its properties are mainly determined by the heat conduction from the corona downwards.

5.1 CORONAL EMISSION AND MAGNETIC STRUCTURE

Coronal loops, as seen in emission originating from gas at around 1 MK (e.g., in a wavelength band near 171 Å), usually emerge from the magnetic concentrations in an active region and appear roughly semicircular with lengths of around 100 Mm and reaching heights of often 50 Mm or more. Mostly, one footpoint of these loops is in the penumbra around the dark core of the sunspot. In a sunspot group, typically the other footpoint is not, as one might expect, at the other sunspot, but found in a plage region of opposite magnetic polarity, i.e., inside the region around the other sunspot with enhanced magnetic flux density. Observations can also show plasma

at higher temperatures above 7 MK, e.g., in X-rays or in a band near 94 Å that contains emission lines of Fe XVIII. These reveal a structure different from what is seen at around 1 MK. Here, the active region is more compact, with shorter loops mostly connecting the sunspots: hence, the term "hot core of an active region." An overview of the appearance of the corona is shown in Fig. 3.1. We come back to a physics-based interpretation of this appearance in Section 5.3, and for the moment discuss only some basic properties of coronal loops.

To test whether the coronal emission that is visible in the form of loops really outlines the magnetic field, one can extrapolate the magnetic field from the photosphere into the upper atmosphere. Direct measurements of the coronal magnetic field are available only above the limb in coronagraphic observations (Lin et al., 2004; Raouafi, 2005), which provide only poor spatial and temporal resolution (because of the limitation of the photon flux). Thus, extrapolations are the major tool for exploring the magnetic structure of the upper atmosphere. Naturally, the magnetic field $\mathbf{B}$ is solenoidal, i.e., $\nabla \times \mathbf{B} = 0$. If we now assume that in the corona there are no (or negligible) currents, $\mathbf{j} \propto \nabla \times \mathbf{B}$, the magnetic field would also be irrotational, $\nabla \times \mathbf{B} = 0$. Consequently, $\mathbf{B}$ can be represented by the gradient of a scalar potential field, $\mathbf{B} = \nabla\Phi$. Hence, this particular case is called the potential magnetic field and has to satisfy $\Delta\Phi = 0$. The solution of this Laplace equation in any given volume depends on the boundary conditions only. Thus, knowledge of the magnetic field at the solar surface is sufficient to determine the magnetic field throughout the whole atmosphere (e.g., assuming periodic boundary conditions in the horizontal direction and $\mathbf{B} = 0$ at infinity). More complex (and, it is hoped, more realistic) forms of magnetic extrapolations exist (Feng et al., 2007). Using these, one can show that indeed the coronal loops seen in observations match the field lines derived from the magnetic field from the extrapolations well (Feng et al., 2007; Wiegelmann et al., 2005).

Typically, the overall appearance of coronal loops evolves on timescales of about 30 min to 1 h. This is much longer than the typical cooling time expected from the energy losses through optically thin radiation (mostly in the extreme UV) and through heat conduction back to the cooler lower atmosphere (Aschwanden, 2004). Therefore, there needs to be a continuous energy input, and the bulk of the coronal loops cannot be understood through a single short heating pulse (Warren et al., 2003). Of course, also much faster small-scale variations are seen on timescales down to a few seconds. Probably these are a direct response to small heating events (Régnier et al., 2014).

The emission in the extreme UV is seen all the way to the apex of loops at heights of 50 Mm or more, which is almost a tenth of a solar radius. However, the barometric scale height at 1 MK in fully ionized hydrogen plasma is 50 Mm. Therefore, one would expect to see a considerable drop in the emission (which is proportional to the density squared). However, that is not the case (Aschwanden et al., 2001). Thus, these loops cannot be in hydrostatic equilibrium, but have to be overdense. This might be achieved through the flow dynamics of the loops and their temporal evolution (Müller et al., 2003), but it is not yet fully understood.

5.2 BASIC CONSIDERATIONS OF THE ENERGETICS

In the corona, the magnetic field energetically dominates the gas, and thus it has to be space filling. The field lines then basically act as a tube to define the coronal loop in which the plasma can move only along but not across the field. Therefore, as a first approximation, one can consider the problem of a coronal loop in only one dimension (along a field line).

Figuratively speaking, the basic question is then why we see one field line highlighted by coronal extreme UV emission while the neighboring field line is dark. We will see that this is determined solely by the energy input.

Consider a loop in equilibrium between energy input, radiative losses, and heat conduction. In a thought experiment, we now increase the energy input, and naturally the temperature rises. At high temperatures, radiative losses are smaller than the loss through heat conduction back to the Sun. So, the additional energy is conducted back to the Sun. There, in the low corona (and upper chromosphere), the plasma becomes heated and evaporates into the loop. This increases the density in the loop. At the same time, the base of the corona moves downward to higher densities (because the very top of the chromosphere was evaporated) and thus the radiative losses at the coronal base increase as well. So, the loop finds a new equilibrium between energy input, heat conduction along the loop, and radiation at its base. So essentially, increasing the energy input results in a higher temperature, but also in a higher density (and thus pressure). Therefore, heating a set of field lines increases the coronal radiation from the plasma trapped between them and they appear as a coronal loop.

This equilibrium of the loop can be described mathematically through scaling laws (Rosner et al., 1978; Priest, 1982) that connect the energy flux F_H into the corona and the loop length L to the resulting temperature T and pressure or number density n (Peter et al., 2012):

$$T[K] = 1700\left(F_H\left[W/m^2\right]\right)^{2/7}(L[m])^{2/7}, \tag{3.1}$$

$$n\left[cm^{-3}\right] = 3.9 \times 10^{10}\left(F_H\left[W/m^2\right]\right)^{4/7}(L[m])^{-3/7}. \tag{3.2}$$

One important corollary is that the heat input sets both the temperature and the density. This implies that for a given loop, one is not free to select the temperature and density independently, but (in equilibrium) they are both set by the energy input (and loop length), and hence they are not independent.

The weak dependence of the temperature on the energy input is because of the high sensitivity of the heat conduction flux on the temperature. The heat conduction in a fully ionized gas is given though $q \propto T^{5/2}\nabla T$ (Spitzer, 1962). Therefore, increasing the temperature just slightly results in a strong increase in heat conduction. In other words, increasing the heating results in a significant enhancement of the heat conduction (carrying away most of the additional heat) and only a small amount of energy is left for only a modest temperature increase: the heat conduction acts like a thermostat.

The requirements for the average heating of the corona have been derived from early extreme UV and x-ray observations through the radiative losses. These gave values for the required energy flux into the upper atmosphere in the quiet Sun corona of about 100 W/m^2 and some 10^4 W/m^2 in an active region (Withbroe and Noyes, 1977). Employing these scaling laws, for a 100-Mm-long loop, this yields temperatures of about 1 and 5 MK, values that are consistent with modern observations (Landi and Feldman, 2008).

5.3 HEATING PROCESSES AND MODERN MODELS

Knowing the requirement for the energy input, this still leaves the questions of where the energy is originating, how it is transported, and how it is finally dissipated. Generally, one distinguishes AC and DC heating, termed after alternating and direct currents. In both cases, the magnetic field at the coronal base (or in the photosphere) is driven by the motions in the photosphere, which essentially leads to a Poynting flux, i.e., a flux of electromagnetic energy, into the upper atmosphere. The magnitude of this flux has to match the requirements in the preceding subsection to sustain a corona.

The driving (or stressing) of the magnetic field induces a perturbation of the magnetic field that propagates essentially with the Alfvén speed, i.e., the speed of a transversal wave of the magnetic field (see Chapter 7 and Priest, 1982). If the driving is faster than the Alfvén speed, the perturbation will be a wave, similar to a piece of rope held in one hand and moved back and forth quickly. The changes of the magnetic field go along with changing induced currents, hence the term "AC." The driving motion can be linear or torsional and will launch a range of waves into the upper atmosphere (van Ballegooijen et al., 2011). If the driving is slower than the Alfvén speed, one simply stresses the magnetic field. If the driving occurs in a randomized fashion (through the motion of the footpoints, e.g., owing to photospheric convection), figuratively speaking, one is braiding the magnetic field lines. The induced currents will not change in a wave fashion, and hence the term "DC." The braiding will build up increasingly stronger currents until a (secondary) instability sets in and releases the energy in a process termed nanoflaring (Parker, 1972, 1988).

Often AC and DC heating are treated as an either/or problem, but on the Sun we expect a wide range of driving timescales. Therefore, wherever there is strong DC heating, one also expects increased AC heating, and vice versa. The energy input in a model that is based on DC or AC heating alone should therefore be considered as a lower limit only, because one might expect both mechanisms to be operational. In the end, what really matters is the magnitude of the Poynting flux into the upper atmosphere used to energize the plasma.

Three-dimensional MHD models have become available that solve the problem of the driving of the corona based on the motions in the photosphere in numerical experiments (Gudiksen and Nordlund, 2002). These showed that indeed, the driving at the solar surface caused a braiding-type effect that can sustain a loop-dominated million-K hot corona (Gudiksen and Nordlund, 2005) and these models match solar

observations in many aspects (Peter et al., 2004). Such 3D models give a good understanding of the observed Doppler shifts (Peter et al., 2006; Solanki et al., 2017), show that most of the energy is dissipated low in the atmosphere in thin current sheet-like structures aligned with the magnetic field (Bingert and Peter, 2011), provide some understanding of the observed constant width of coronal loops (Peter and Bingert, 2012), and show the clear relation of the increased Poynting flux at the base of the corona with the appearance of bright loops (Chen et al., 2015), to name a few. The last result also clarifies why loops are not rooted in the center of a sunspot, the dark umbra. There, the magnetic field is so strong that it suppresses the (convective) horizontal motions in the photosphere to a large extent. Consequently, in the umbra, the Poynting flux is low, whereas it is high in the region of the penumbra (Chen et al., 2014), and the loops are primarily rooted in the penumbra if they come close to a sunspot.

One key ingredient of these 3D MHD models is the inclusion of heat conduction. Only then are the temperature and density of the corona set properly (see Section 5.2). This is a prerequisite to derive the coronal emission. The emission from the corona is optically thin and dominated by emission lines from highly ionized species. In general, the excitation of these lines is caused by electron collisions, and mostly the de-excitation is the result of spontaneous emission. Spontaneous emission is much faster than collisional excitation; hence, all ions are in the ground state almost all of the time. Because of the electron collisional excitation, the emissivity is (roughly) proportional to the density squared. Mostly the assumption of ionization equilibrium, mediated by electron collisions, is justified (Chen et al., 2014), and the typical ionization stages are restricted to a narrow range in plasma temperature (typically over $\log T[K] \approx 0.2$, i.e., a factor of 1.5). This is why we can consider that a narrow extreme UV band dominated by one emission line provides information about the distribution of plasma in a narrow temperature range, e.g., why the 171 Å band dominated by Fe IX shows plasma at around 1 MK.

5.4 CONNECTION TO THE LOW ATMOSPHERE

Of course, the corona has to be magnetically connected to (or rooted in) the photosphere. However, finding a clear correspondence between coronal intensity structures, such as loops, and features of the magnetic field in the photosphere is extremely challenging. One reason for this is the significant difference in spatial resolution of observations, which typically is a factor of five or more worse in the corona compared with in the photosphere. The workhorse of coronal observations, the AIA (Lemen et al., 2012), provides a plate scale of 0.6 arcsec per pixel and a spatial resolution of about 1.4 arcsec. On a rocket flight, the High-resolution Coronal imager could provide a few minutes' worth of coronal images at 0.3−0.4 arcsec resolution (Cirtain et al., 2013) and the Interface Region Imaging Spectrograph (De Pontieu et al., 2014) regularly provides about 0.35 arcsec resolution, although it concentrates on the chromosphere and the transition region into the corona. These resolutions are considerably lower than those obtained in photospheric and

chromospheric observations achieved by the SUNRISE balloon observatory (Solanki et al., 2017) or ground-based solar observatories with apertures of up to 1.5 m that can go town to 50 km on the Sun.

Despite this mismatch in spatial resolution, one can patch together observations from the photosphere, chromosphere, and corona to study the connectivity. One of the most enigmatic features in the solar atmosphere is spicules and what drives them. Reported already by Secchi in the late 19th century, they are well-investigated observationally, but their physics is poorly understood. In spicules, plasma is propelled upward, best seen in the emission of Hα. In one type (I), the chromospheric plasma follows a ballistic trajectory, eventually falling back to the Sun; in another type (II), they seem simply to dissolve in Hα (de Pontieu et al., 2007), which probably is a signature of heating of the plasma (Pereira et al., 2014). It has been suggested that ambipolar diffusion has a critical role (Martínez-Sykora et al., 2017). Then the magnetic field can emerge more efficiently from the photosphere upward (in slipping through the partially ionized plasma). This then leads to more vigorous reconnection driving the spicules.

An important aspect of connecting the coronal structures to the photospheric magnetic field concerns the response of the corona to changes in the connectivity of the magnetic field deep in the photosphere and chromosphere. Observations established the important role of reconnection at height levels where the chromosphere would normally be located (Peter et al., 2014). In particular, one could track extreme UV brightenings and relate them to reconnection sites (determined by magnetic extrapolations) that were located only some 500 km above the photosphere (Chitta et al., 2017a), i.e., near the temperature minimum (see Fig. 3.3). Comparing coronal data with the high-resolution photospheric magnetic field in more detail shows that loops are rooted at locations of small-scale mixed polarities (Chitta et al., 2017b). This highlights the importance of reconnection in the chromosphere for the heating the corona. Thus, besides AC and DC heating discussed in Section 5.3, this an adds a third path to coronal energization, which needs to be explored in the future.

ACKNOWLEDGMENTS

This project has received funding from the European Research Council under the European Unions Horizon 2020 research and innovation program (Grant Agreement Nos. 624817 and 695075) and was supported by the BK21 Plus program through the National Research Foundation funded by the Ministry of Education of Korea.

REFERENCES

Allende Prieto, C., Asplund, M., García López, R.J., et al., 2002. Signatures of convection in the spectrum of Procyon: fundamental parameters and iron abundance. Astrophys. J. 567, 544−565. https://doi.org/10.1086/338248. astro-ph/0111055.

Aschwanden, M.J., Schrijver, C.J., Alexander, D., 2001. Modeling of coronal EUV loops observed with TRACE. I. Hydrostatic solutions with nonuniform heating. Astrophys. J. 550, 1036−1050. https://doi.org/10.1086/319796.

Aschwanden, M.J., 2004. Physics of the Solar Corona. An Introduction. Praxis Publishing Ltd.

Asplund, M., Nordlund, Å., Trampedach, R., et al., 1999. 3D hydrodynamical model atmospheres of metal-poor stars. Evidence for a low primordial Li abundance. Astron. Astrophys. 346, L17−L20. astro-ph/9905059.

Avrett, E.H., 1985. Recent thermal models of the chromosphere. In: Lites, B.W. (Ed.), Chromospheric Diagnostics and Modelling, pp. 67−127.

Beeck, B., Cameron, R.H., Reiners, A., et al., 2013. Three-dimensional simulations of near-surface convection in main-sequence stars. I. Overall structure. Astron. Astrophys. 558, A48. https://doi.org/10.1051/0004−6361/201321343. 1308.4874.

Beeck, B., Schüssler, M., Cameron, R.H., et al., 2015. Three-dimensional simulations of near-surface convection in main-sequence stars. III. The structure of small-scale magnetic flux concentrations. Astron. Astrophys. 581, A42. https://doi.org/10.1051/0004−6361/201525788. 1505.04739.

Bingert, S., Peter, H., 2011. Intermittent heating in the solar corona employing a 3D MHD model. Astron. Astrophys. 530, A112. https://doi.org/10.1051/0004−6361/201016019. 1103.6042.

Böhm-Vitense, E., 1958. Über die Wasserstoffkonvektionszone in Sternen verschiedener Effektivtemperaturen und Leuchtkräfte. Mit 5 Textabbildungen. Z. Astrophys. 46, 108.

Brault, J.W., 1985. Fourier transform spectroscopy. In: Benz, A.O., Huber, M., Mayor, M. (Eds.), High Resolution in Astronomy, Fifteenth Advanced Course of the Swiss Society of Astronomy and Astrophysics. Geneva Observatory, Sauverny, Switzerland, pp. 3−61.

Carlsson, M., Leenaarts, J., 2012. Approximations for radiative cooling and heating in the solar chromosphere. Astron. Astrophys. 539, A39. https://doi.org/10.1051/0004−6361/201118366. 1202.2996.

Carlsson, M., Stein, R.F., Nordlund, Å., et al., 2004. Observational manifestations of solar magnetoconvection: center-to-limb variation. Astrophys. J. Lett. 610, L137−L140. https://doi.org/10.1086/423305. astro-ph/0406160.

Castelli, F., Gratton, R.G., Kurucz, R.L., 1997. Notes on the convection in the ATLAS9 model atmospheres. Astron. Astrophys. 318, 841−869.

Chen, F., Peter, H., Bingert, S., et al., 2014. A model for the formation of the active region corona driven by magnetic flux emergence. Astron. Astrophys. 564, A12. https://doi.org/10.1051/0004−6361/201322859. 1402.5343.

Chen, F., Peter, H., Bingert, S., et al., 2015. Magnetic jam in the corona of the Sun. Nat. Phys. 11, 492−495. https://doi.org/10.1038/nphys3315. 1505.01174.

Chitta, L.P., Peter, H., Young, P.R., et al., 2017a. Compact solar UV burst triggered in a magnetic field with a fan-spine topology. Astron. Astrophys. 605, A49. https://doi.org/10.1051/0004−6361/201730830. 1706.08059.

Chitta, L.P., Peter, H., Solanki, S.K., et al., 2017b. Solar coronal loops associated with small-scale mixed polarity surface magnetic fields. ApJS 229, 4. https://doi.org/10.3847/1538-4365/229/1/4. 1610.07484.

Cirtain, J.W., Golub, L., Winebarger, A.R., et al., 2013. Energy release in the solar corona from spatially resolved magnetic braids. Nature 493, 501−503. https://doi.org/10.1038/nature11772.

de la Cruz Rodríguez, J., Leenaarts, J., Asensio Ramos, A., 2016. Non-lte inversions of the Mg II h k and UV triplet lines. Astrophys. J. Lett. 830, L30. https://doi.org/10.3847/2041-8205/830/2/L30. 1609.09527.

de Laverny, P., Recio-Blanco, A., Worley, C.C., et al., 2012. The AMBRE project: a new synthetic grid of high-resolution FGKM stellar spectra. Astron. Astrophys. 544, A126. https://doi.org/10.1051/0004−6361/201219330. 1205.2270.

de Pontieu, B., McIntosh, S., Hansteen, V.H., et al., 2007. A tale of two spicules: the impact of spicules on the magnetic chromosphere. Publ. Astron. Soc. Jpn. 59, S655−S662. https://doi.org/10.1093/pasj/59.sp3.S655. 0710.2934.

De Pontieu, B., Title, A.M., Lemen, J.R., et al., 2014. The interface region imaging Spectrograph (IRIS). Sol. Phys. 289, 2733−2779. https://doi.org/10.1007/s11207-014-0485-y. 1401.2491.

Doerr, H.-P., Vitas, N., Fabbian, D., 2016. How different are the Liège and Hamburg atlases of the solar spectrum? Astron. Astrophys. 590, A118. https://doi.org/10.1051/0004−6361/201628570. 1604.03748.

Ermolli, I., Matthes, K., Dudok de Wit, T., et al., 2013. Recent variability of the solar spectral irradiance and its impact on climate modelling. Atmos. Chem. Phys. 13, 3945−3977. https://doi.org/10.5194/acp-13-3945-2013. 1303.5577.

Feng, L., Inhester, B., Solanki, S.K., et al., 2007. First stereoscopic coronal loop reconstructions from STEREO SECCHI images. Astrophys. J. Lett. 671, L205−L208. https://doi.org/10.1086/525525. 0802.0773.

Fontenla, J.M., Avrett, E.H., Loeser, R., 1993. Energy balance in the solar transition region. III - helium emission in hydrostatic, constant-abundance models with diffusion. Astrophys. J. 406, 319−345. https://doi.org/10.1086/172443.

Fontenla, J., White, O.R., Fox, P.A., et al., 1999. Calculation of solar irradiances. I. Synthesis of the solar spectrum. Astrophys. J. 518, 480−499. https://doi.org/10.1086/307258.

Fontenla, J.M., Stancil, P.C., Landi, E., 2015. Solar spectral irradiance, solar activity, and the near-ultra-violet. Astrophys. J. 809, 157. https://doi.org/10.1088/0004-637X/809/2/157.

Freytag, B., Ludwig, H.-G., Steffen, M., 1996. Hydrodynamical models of stellar convection. The role of overshoot in DA white dwarfs, A-type stars, and the Sun. Astron. Astrophys. 313, 497−516.

Frutiger, C., Solanki, S.K., Fligge, M., et al., 2000. Properties of the solar granulation obtained from the inversion of low spatial resolution spectra. Astron. Astrophys. 358, 1109−1121.

Golding, T.P., Leenaarts, J., Carlsson, M., 2016. Non-equilibrium helium ionization in an MHD simulation of the solar atmosphere. Astrophys. J. 817, 125. https://doi.org/10.3847/0004-637X/817/2/125. 1512.04738.

Gudiksen, B.V., Nordlund, Å., 2002. Bulk heating and slender magnetic loops in the solar corona. Astrophys. J. Lett. 572, L113−L116. https://doi.org/10.1086/341600.

Gudiksen, B.V., Nordlund, Å., 2005. An AB initio approach to solar coronal loops. Astrophys. J. 618, 1031−1038. https://doi.org/10.1086/426064. astro-ph/0407267.

Gustafsson, B., Edvardsson, B., Eriksson, K., et al., 2008. A grid of MARCS model atmospheres for late-type stars. I. Methods and general properties. Astron. Astrophys. 486, 951−970. https://doi.org/10.1051/0004-6361:200809724. 0805.0554.

Hatzes, A.P., 2016. The radial velocity method for the detection of exoplanets. In: Bozza, V., Mancini, L., Sozzetti, A. (Eds.), Methods of Detecting Exoplanets: 1st Advanced School on Exoplanetary Science. In: Astrophysics and Space Science Library, vol. 428, p. 3. https://doi.org/10.1007/978-3-319-27458-41.

Hayek, W., Asplund, M., Carlsson, M., et al., 2010. Radiative transfer with scattering for domain-decomposed 3D MHD simulations of cool stellar atmospheres. Numerical methods and application to the quiet, non-magnetic, surface of a solar-type star. Astron. Astrophys. 517, A49. https://doi.org/10.1051/0004−6361/201014210. 1007.2760.

Hubeny, I., Mihalas, D., 2014. Theory of Stellar Atmospheres. Princeton University Press.

Husser, T.-O., Wende-von Berg, S., Dreizler, S., et al., 2013. A new extensive library of PHOENIX stellar atmospheres and synthetic spectra. Astron. Astrophys. 553, A6. https://doi.org/10.1051/0004−6361/201219058. 1303.5632.

Jafarzadeh, S., Solanki, S.K., Cameron, R.H., et al., 2017. Kinematics of magnetic bright features in the solar photosphere. ApJS 229, 8. https://doi.org/10.3847/1538-4365/229/1/8. 1610.07634.

Joshi, J., Pietarila, A., Hirzberger, J., et al., 2011a. Convective nature of sunspot penumbral filaments: discovery of downflows in the deep photosphere. Astrophys. J. Lett. 734, L18. https://doi.org/10.1088/2041-8205/734/1/L18. 1105.1877.

Joshi, J., Pietarila, A., Hirzberger, J., Solanki, S.K., Aznar Cuadrado, R., Merenda, L., 2011b. Convective Nature of Sunspot Penumbral Filaments: Discovery of Downflows in the Deep Photosphere. Astrophys. J. Lett. 734, L18. https://doi.org/10.1088/2041-8205/734/1/L18. 1105.1877.

Koesterke, L., Allende Prieto, C., Lambert, D.L., 2008. Center-to-Limb variation of solar three-dimensional hydrodynamical simulations. Astrophys. J. 680, 764−773. https://doi.org/10.1086/587471. 0802.2177.

Kurucz, R.L., Furenlid, I., Brault, J., Testerman, L., 1984. Solar Flux Atlas from 296 to 1300 nm.

Kurucz, R.L., 2005a. New atlases for solar flux, irradiance, central intensity, and limb intensity. Mem. Soc. Astron. Ital. Suppl. 8, 189.

Kurucz, R.L., 2005b. Including all the lines. Mem. Soc. Astron. Ital. Suppl. 8, 86.

Kurucz, R.L., 2005c. ATLAS12, SYNTHE, ATLAS9, WIDTH9, et cetera. Mem. Soc. Astron. Ital. Suppl. 8, 14.

Lagg, A., Solanki, S.K., Riethmüller, T.L., et al., 2010. Fully resolved quiet-sun magnetic flux tube observed with the SUNRISE/IMAX Instrument. Astrophys. J. Lett. 723, L164−L168. https://doi.org/10.1088/2041-8205/723/2/L164. 1009.0996.

Lagg, A., Solanki, S.K., Doerr, -P., et al., 2016. Probing deep photospheric layers of the quiet Sun with high magnetic sensitivity. Astron. Astrophys. 596, A6. https://doi.org/10.1051/0004−6361/201628489. 1605.06324.

Landi, E., Feldman, U., 2008. The thermal structure of an active region observed outside the solar disk. Astrophys. J. 672, 674−683. https://doi.org/10.1086/523629.

Lemen, J.R., Title, A.M., Akin, D.J., et al., 2012. The atmospheric imaging assembly (AIA) on the solar dynamics observatory (SDO). Sol. Phys. 275, 17−40. https://doi.org/10.1007/s11207-011-9776-8.

Lin, H., Kuhn, J.R., Coulter, R., 2004. Coronal magnetic field measurements. Astrophys. J. Lett. 613, L177−L180. https://doi.org/10.1086/425217.

Liseau, R., Montesinos, B., Olofsson, G., et al., 2013. α Centauri A in the far infrared. First measurement of the temperature minimum of a star other than the Sun. Astron. Astrophys. 549, L7. https://doi.org/10.1051/0004−6361/201220776. 1212.3954.

Martínez-Sykora, J., De Pontieu, B., Hansteen, V.H., et al., 2017. On the generation of solar spicules and Alfvénic waves. Science 356, 1269−1272. https://doi.org/10.1126/science.aah5412. 1710.07559.

Müller, D.A.N., Hansteen, V.H., Peter, H., 2003. Dynamics of solar coronal loops. I. Condensation in cool loops and its effect on transition region lines. Astron. Astrophys. 411, 605−613. https://doi.org/10.1051/0004-6361:20031328.

Nordlund, A., Dravins, D., 1990. Stellar granulation. III - hydrodynamic model atmospheres. IV - line formation in inhomogeneous stellar photospheres. V - synthetic spectral lines in disk-integrated starlight. Astron. Astrophys. 228, 155−217.

Nordlund, Å., Stein, R.F., Asplund, M., 2009. Solar surface convection. Living Rev. Sol. Phys. 6, 2. https://doi.org/10.12942/lrsp-2009-2.

Nordlund, A., 1982. Numerical simulations of the solar granulation. I - basic equations and methods. Astron. Astrophys. 107, 1−10.

Orozco Suárez, D., Bellot Rubio, L.R., del Toro Iniesta, J.C., et al., 2007. Quiet-sun internetwork magnetic fields from the inversion of Hinode measurements. Astrophys. J. Lett. 670, L61−L64. https://doi.org/10.1086/524139. 0710.1405.

Parker, E.N., 1972. Topological dissipation and the small-scale fields in turbulent gases. Astrophys. J. 174, 499. https://doi.org/10.1086/151512.

Parker, E.N., 1988. Nanoflares and the solar X-ray corona. Astrophys. J. 330, 474−479. https://doi.org/10.1086/166485.

Pereira, T.M.D., De Pontieu, B., Carlsson, M., et al., 2014. An interface region imaging Spectrograph first view on solar spicules. Astrophys. J. Lett. 792, L15. https://doi.org/10.1088/2041-8205/792/1/L15. 1407.6360.

Peter, H., Bingert, S., 2012. Constant cross section of loops in the solar corona. Astron. Astrophys. 548, A1. https://doi.org/10.1051/0004−6361/201219473. 1209.0789.

Peter, H., Gudiksen, B.V., Nordlund, Å., 2004. Coronal heating through braiding of magnetic field lines. Astrophys. J. Lett. 617, L85−L88. https://doi.org/10.1086/427168. astro-ph/0409504.

Peter, H., Gudiksen, B.V., Nordlund, Å., 2006. Forward modeling of the corona of the Sun and solar-like stars: from a three-dimensional magnetohydrodynamic model to synthetic extreme-ultraviolet spectra. Astrophys. J. 638, 1086−1100. https://doi.org/10.1086/499117. astro-ph/0503342.

Peter, H., Bingert, S., Kamio, S., 2012. Catastrophic cooling and cessation of heating in the solar corona. Astron. Astrophys. 537, A152. https://doi.org/10.1051/0004−6361/201117889. 1112.3667.

Peter, H., Tian, H., Curdt, W., et al., 2014. Hot explosions in the cool atmosphere of the Sun. Science 346, 1255726. https://doi.org/10.1126/science.1255726. 1410.5842.

Priest, E.R., 1982. Solar Magneto-Hydrodynamics. Dordrecht, Holland; Boston: D. Reidel Pub. Co.; Hingham.

Ramírez, I., Allende Prieto, C., Koesterke, L., et al., 2009. Granulation in K-type dwarf stars. II. Hydrodynamic simulations and 3D spectrum synthesis. Astron. Astrophys. 501, 1087−1101. https://doi.org/10.1051/0004-6361/200911741. 0905.3101.

Raouafi, N.-E., 2005. Measurement methods for chromospheric and coronal magnetic fields. In: Innes, D.E., Lagg, A., Solanki, S.A., (Eds.), Chromospheric and Coronal Magnetic Fields. In: ESA Special Publication, vol. 596, p. 3.1.

Régnier, S., Alexander, C.E., Walsh, R.W., et al., 2014. Sparkling extreme-ultraviolet bright dots observed with Hi-C. Astrophys. J. 784, 134. https://doi.org/10.1088/0004-637X/784/2/134. 1402.2457.

Riethmüller, T.L., Solanki, S.K., Berdyugina, S.V., et al., 2014. Comparison of solar photospheric bright points between Sunrise observations and MHD simulations. Astron. Astrophys. 568, A13. https://doi.org/10.1051/0004−6361/201423892. 1406.1387.

Rosner, R., Tucker, W.H., Vaiana, G.S., 1978. Dynamics of the quiescent solar corona. Astrophys. J. 220, 643−645. https://doi.org/10.1086/155949.

Rutten, R.J., 2002. Solar atmosphere models. J. Astron. Data 8.

Scharmer, G.B., Henriques, V.M.J., Kiselman, D., et al., 2011. Detection of convective downflows in a sunspot penumbra. Science 333, 316. https://doi.org/10.1126/science.1206429.

Schrijver, C.J., Title, A.M., Harvey, K.L., et al., 1998. Large-scale coronal heating by the small-scale magnetic field of the Sun. Nature 394, 152−154. https://doi.org/10.1038/28108.

Schüssler, M., 2001. Numerical simulation of solar magneto-convection. In: Sigwarth, M. (Ed.), Advanced Solar Polarimetry − Theory, Observation, and Instrumentation. In: Astronomical Society of the Pacific Conference Series, vol. 236, p. 343.

Shapiro, A.I., Solanki, S.K., Krivova, N.A., et al., 2015. The role of the Fraunhofer lines in solar brightness variability. Astron. Astrophys. 581, A116. https://doi.org/10.1051/0004−6361/201526483. 1507.05437.

Short, C.I., Hauschildt, P.H., 2009. Non-lte modeling of the near-ultraviolet band of late-type stars. Astrophys. J. 691, 1634−1647. https://doi.org/10.1088/0004-637X/691/2/1634.0811.1145.

Solanki, S.K., Hammer, R., 2002. The Solar Atmosphere. Kluwer Academic Publishers, p. 1065.

Solanki, S.K., Inhester, B., Schüssler, M., 2006. The solar magnetic field. Rep. Progr. Phys. 69, 563−668. https://doi.org/10.1088/0034-4885/69/3/R02. 1008.0771.

Solanki, S.K., Barthol, P., Danilovic, S., et al., 2010. SUNRISE: instrument, mission, data, and first results. Astrophys. J. Lett. 723, L127−L133. https://doi.org/10.1088/2041-8205/723/2/L127. 1008.3460.

Solanki, S.K., Krivova, N.A., Haigh, J.D., 2013. Solar irradiance variability and climate. Ann. Rev. Astron. Astrophys. 51, 311−351. https://doi.org/10.1146/annurev-astro-082812-141007. 1306.2770.

Solanki, S.K., Riethmüller, T.L., Barthol, P., et al., 2017. The second flight of the Sunrise balloon-borne solar observatory: overview of instrument updates, the flight, the data, and first results. ApJS 229, 2. https://doi.org/10.3847/1538-4365/229/1/2. 1701.01555.

Solanki, S.K., 1993. Smallscale solar magnetic fields - an overview. Space Sci. Rev. 63, 1−188. https://doi.org/10.1007/BF00749277.

Spitzer, L., 1962. Physics of Fully Ionized Gases. New York: Interscience (2nd edition).

Stein, R.F., 2012. Solar surface magneto-convection. Living Rev. Sol. Phys. 9, 4. https://doi.org/10.12942/lrsp-2012-4.

Trampedach, R., Asplund, M., Collet, R., et al., 2013. A grid of three-dimensional stellar atmosphere models of solar metallicity. I. General properties, granulation, and atmospheric expansion. Astrophys. J. 769, 18. https://doi.org/10.1088/0004-637X/769/1/18. 1303.1780.

Tremblay, P.-E., Ludwig, H.-G., Freytag, B., et al., 2013. Granulation properties of giants, dwarfs, and white dwarfs from the CIFIST 3D model atmosphere grid. Astron. Astrophys. 557, A7. https://doi.org/10.1051/0004−6361/201321878. 1307.2810.

Uitenbroek, H., Criscuoli, S., 2011. Why one-dimensional models fail in the diagnosis of average spectra from inhomogeneous stellar atmospheres. Astrophys. J. 736, 69. https://doi.org/10.1088/0004-637X/736/1/69. 1101.2643.

van Ballegooijen, A.A., Asgari-Targhi, M., Cranmer, S.R., et al., 2011. Heating of the solar chromosphere and corona by Alfvén wave turbulence. Astrophys. J. 736, 3. https://doi.org/10.1088/0004-637X/736/1/3. 1105.0402.

Vernazza, J.E., Avrett, E.H., Loeser, R., 1981. ApJS 45, 635.
Vitas, N., Khomenko, E., 2015. Equation of state for solar near-surface convection. Ann. Geophys. 33, 703−709. https://doi.org/10.5194/angeo-33-703-2015.
Vögler, A., Shelyag, S., Schüssler, M., et al., 2005. Simulations of magneto-convection in the solar photosphere. Equations, methods, and results of the MURaM code. Astron. Astrophys. 429, 335−351. https://doi.org/10.1051/0004-6361:20041507.
Wallace, L., Hinkle, K.H., Livingston, W.C., et al., 2011. An optical and near-infrared (2958-9250 Å) solar flux atlas. ApJS 195, 6. https://doi.org/10.1088/0067-0049/195/1/6.
Warren, H.P., Winebarger, A.R., et al., 2003. Evolving active region loops observed with the transition region and coronal explorer. II. Time-dependent hydrodynamic simulations. Astrophys. J. 593, 1174−1186. https://doi.org/10.1086/376678.
Werner, K., Deetjen, J.L., Dreizler, S., Nagel, T., Rauch, T., Schuh, S.L., 2003. Model photospheres with accelerated lambda iteration. In: Hubeny, I., Mihalas, D., Werner, K. (Eds.), Stellar Atmosphere Modeling. In: Astronomical Society of the Pacific Conference Series, vol. 288. p. 31. astro-ph/0209535.
Wiegelmann, T., Lagg, A., Solanki, S.K., et al., 2005. Comparing magnetic field extrapolations with measurements of magnetic loops. Astron. Astrophys. 433, 701−705. https://doi.org/10.1051/0004-6361:20042421. 0801.4519.
Wiegelmann, T., Thalmann, J.K., Solanki, S.K., 2014. The magnetic field in the solar atmosphere. Astron. Astrophys. Rev. 22, 78. https://doi.org/10.1007/s00159-014-0078-7. 1410.4214.
Withbroe, G.L., Noyes, R.W., 1977. Mass and energy flow in the solar chromosphere and corona. Ann. Rev. Astron. Astrophys. 15, 363−387. https://doi.org/10.1146/annurev.aa.15.090177.002051.

The Sun as a Guide to Stellar Physics

An up-to-date view of the field of solar physics, illustrating the significance of the Sun as a guide star in understanding stellar astrophysics and related fields

- Applies observations, theoretical understanding, modeling capabilities, and physical processes first revealed by the Sun to the study of stellar physics
- Illustrates how studies of 'proxima solaris' have led to progress in space science, stellar physics, and other related fields
- Uses characteristics of solar phenomena as a guide to understanding the physics of stars

The Sun as a Guide to Stellar Physics illustrates the significance of the Sun in understanding stars through an examination of the discoveries and insights gained from solar physics research. Ranging from theories to modeling and from numerical simulations to instrumentation and data processing, the book provides an overview of what we currently understand and how the Sun can be a model for gaining further knowledge about stellar physics. Providing both updates on recent developments in solar physics and applications to stellar physics, this book strengthens the solar–stellar connection and summarizes what we know about the Sun for the stellar, space, and geophysics communities.

Contributors include: Tom Ayres, Gibor Basri, Sarbani Basu, Bill Chaplin, Oddbjørn Engvold, Marianne Faurobert, Petr Heinzel, Hugh Hudson, Neal Hurlburt, Kiyoshi Ichimoto, Phil Judge, BC Low, Noé Lugaz, Alec MacKinnon, Hardi Peter, Eric Priest, Alexander Shapiro, Andrew Skumanich, Sami Solanki, Alan Title, Jean-Claude Vial, and Jack Zirker

Oddbjørn Engvold, Professor Emeritus, Institute of Theoretical Astrophysics and Rosseland Centre for Solar Physics, University of Oslo, Norway

Jean-Claude Vial, Senior Scientist Emeritus, Institut d'Astrophysique Spatiale, CNRS-Université Paris-Sud, France

Andrew Skumanich, Senior Scientist Emeritus, High Altitude Observatory, National Center for Atmospheric Research, United States

elsevier.com/books-and-journals

ISBN 978-0-12-814334-6

9 780128 143346